Surface & Coatings Technology 344 (2018) 295–302

Contents lists available at ScienceDirect

Surface & Coatings Technology

journal homepage: www.elsevier.com/locate/surfcoat

Insights into formation of gradient nanostructured (GNS) layer and deformation induced martensite in AISI 316 stainless steel subjected to severe shot peening

M. Jayalakshmi[a], Prashant Huilgol[a], Badekai Ramachandra Bhat[b], K. Udaya Bhat[a,*]

[a] Dept. of Metallurgical and Materials Engineering, National Institute of Technology Karnataka, Surathkal, Karnataka 575025, India
[b] Dept. of Chemistry, National Institute of Technology Karnataka, Surathkal, Karnataka 575025, India

ARTICLE INFO

Keywords:
Severe peening
Deformation induced martensite
Shear bands
Surface nanocrystallization
Transmission electron microscopy

ABSTRACT

Severe peening is a well-accepted top-down approach to engender surface nanocrystallization in austenitic stainless steels. In the present study, AISI 316 grade austenitic stainless steel is subjected to severe peening through air blast shot peening technique. Study is aimed at analyzing the microstructural features of the peened layer and deformation induced martensite through transmission electron microscopy technique. Gradient nanostructured (GNS) layer formed as a result of high strain rate, multi-directional deformation during severe peening found to extend to about 500 μm from the surface. Nucleation of deformation induced martensite is not limited to shear band intersections as affirmed by the published literature related to severe peening. It is observed to nucleate at multiple locations in the austenite matrix. Martensite units thus formed, coalesce with each other to form continuous layer of lath martensite layer at about 15–20 μm from the surface. Upon further deformation, lath morphology transforms to dislocation cell-type; resulting in fine martensite crystallites at the topmost layer of the peened surface.

1. Introduction

Severe peening (through air blast shot peening, laser peening, ultrasonic peening, etc.) is an important top-down approach to obtain nanostructured layer in metals and alloys [1–5]. Advantages of this technique include precise control of process variables, industrial adaptability and cost-effectiveness. Nano-scale/ultra-fine grain structure evolves during the process along with large defect density; which collectively enhance the hardness and wear resistance of the surface. Peening is also extensively employed as a pre-treatment step in diffusion based surface modification techniques like nitriding [6], carburizing [7], nitro-carburizing [8], boronizing [9], etc., to enhance the diffusion kinetics.

Severe peening of the austenitic stainless steels is widely studied owing to the technological significance of these alloys. When implemented as a pre-treatment step, severe peening significantly enhances the diffusion kinetics [6,10] apart from improving the mechanical properties of austenitic steel [11]. Microstructural evolution during severe peening is complex as the process generates gradient nano-structured (GNS) [12–14] layer having layers of differential microstructural features. Deformation induced transformation of austenite to martensite further increases the complexity.

Mechanism of nanocrystallization and martensitic transformation upon severe peening is still a matter of debate amongst the researchers. During ultrasonic peening of the 316L SS, Liu et al. [4] observed that dislocation activity driven by intense localized stress is responsible for the grain refinement through subgrain formation. It was supported by the work of Chen et al. [15]; in which ultrasonic peening of 304SS at strain rate below $10^3\,s^{-1}$ was studied. Detailed microstructural investigation of 304 SS subjected to SMAT was carried out by Zhang et al. [16] through electron microscopy technique. It was inferred that the twin-twin intersections repeatedly sub-divide the austenite grains and also act as nucleation sites for martensitic transformation. Closer to the surface, intersecting twins become finer in dimension leading to the formation of nano-sized martensite crystallites having random orientations. Lu et al. [5] suggested that during laser shock peening of 304 SS, grain sub-division by deformation twinning and continuous dynamic recrystallization (DRX) is responsible for nanocrystallization. Deformation induced martensite (DIM) formation was not observed in the study. However, Zhou et al. [17] opine that the mechanical twins as well as DIM are equally responsible for grain refinement process during laser shock peening of 304SS. Bhagerifard et al. [11] studied the severe

* Corresponding author.
E-mail address: udayabhatk@gmail.com (K. Udaya Bhat).

https://doi.org/10.1016/j.surfcoat.2018.03.028
Received 17 November 2017; Received in revised form 20 February 2018; Accepted 12 March 2018
Available online 13 March 2018
0257-8972/

shot peening of 316 L SS and observed that, upon peening, the layers DIM gets embedded in the austenite matrix. Defect density was observed to decrease due to dynamic annealing and geometric DRX. Recent report by Bahl et al. [18] suggested that microbands and shear bands are formed during the SMAT of 316L SS. Deformation twinning and DRX within the shear bands are responsible for nanocrystallization.

In the recent study by the authors, severe shot peening was successfully used as the pre-treatment step for low temperature plasma nitriding of 316 SS [19]. Upon severe peening, it was observed that about 500 μm depth from the top surface was affected by the peening process. Martensite phase with dislocation cell type morphology was observed on the top surface with a cell size in the range of 100–140 nm. Well-developed, complete layer of lath martensite was found beneath. It was observed at a depth of about 20 μm from the peened surface. The region beneath that was consisting of deformation features [20]. Significant improvement in the case depth was observed after plasma nitriding treatment; owing to higher defect density in the peened layer. Evolution of the microstructural features during severe peening was distinctly different from the reported literature. Formation of continuous layer of lath martensite was not observed in the previous reports on severe peening; despite the fact that it is the dominant martensite morphology in strain induced transformation of austenitic stainless steels. These observations were intuitive to carry out a detailed microstructural investigation to acquire insights into evolution of gradient nanostructured layer and martensitic transformation upon severe peening. Hence, in the present study, peened layer of 316 SS subjected to severe air blast shot peening is studied through transmission electron microscopy technique.

2. Experimental details

Hot-rolled AISI 316 grade stainless steel sheet of 5 mm thickness is used in the study. Composition of the steel is given in Table 1. The microstructure of the alloy is fully austenitic; with grain size in the range of 40–80 μm. Deformation induced martensite is absent in the as-received condition.

Specimens are subjected to air blast shot peening (M/s Curtiss Wright surface technologies, Bangalore) at an Almen intensity of 8A. Peening coverage of 1000% is maintained to ensure severe peening. Cast steel balls (S230) of diameter 0.6 mm were used for the shot peening process at a shot flow velocity of 25 kg/min. Details of the process parameters are given in the reference [20]. Microstructural investigation of the severe peened sample is carried out using scanning electron microscope (SEM, 6380LA, JEOL) operating at 20 kV and transmission electron microscope (TEM, JEM-2100, JEOL) operating at 200 kV. Samples for transmission electron microscopy studies are prepared by initially cutting 1 mm slices of the material from the peened surface by electric discharge machining process. Samples were subjected to mechanical thinning from either the untreated side (for the top surface sample) or from both the sides (for sub-surface samples) to the site of interest by mechanical thinning. 3 mm disks are punched and further thinned to 80 μm thickness. Samples are dimpled to a thickness to about 5 μm at the center. Finally, samples are thinned down to electron transparency limit by ion milling technique. Milling is done using Gatan PIPS system operated at an accelerating voltage of 5 kV and angle of 5°.

3. Results and discussion

Severe shot peening generates gradient nano-structured (GNS) layer consisting of gradient of microstructural features from the unaffected base metal to the severely peened top surface. Cross-sectional SEM micrograph of severe peened 316 SS is shown in Fig. 1. It could be observed that the GNS layer is broadly classified into (a) nanocrystalline region extending to about 20 μm from the top surface and (b) transition region extending beneath. It is observed in the reported work [20] of the authors that nanocrystalline region consists of only martensite phase while the transition region is composed of both, martensite and austenite phases. It is also observed that the transition region extends to about 500 μm from the top surface.

Table 1
Composition of the 316 SS.

Element	Cr	Ni	C	Mn	Mo	Si	S	Fe
Amount (wt%)	17.8	11.5	0.07	1.58	2.08	0.04	0.006	Balance

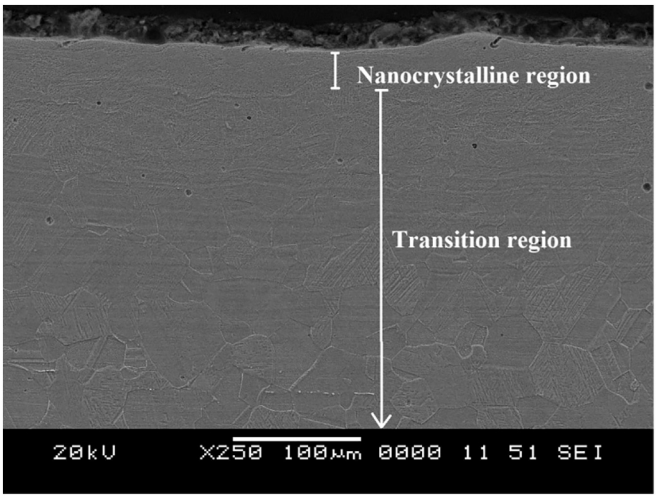

Fig. 1. Cross-sectional SEM micrograph of severe peened 316SS showing gradient nanostructure layer.

Detailed microstructural investigation across the cross-section of the peened specimen is carried out using transmission electron microscopy technique and the results provided insights about the martensitic transformation and surface nanocrystallization.

3.1. Microstructure below the GNS layer

Typical bright field TEM micrograph below the GNS layer (more than 500 μm away from the top surface) is shown in Fig. 2. Large grains

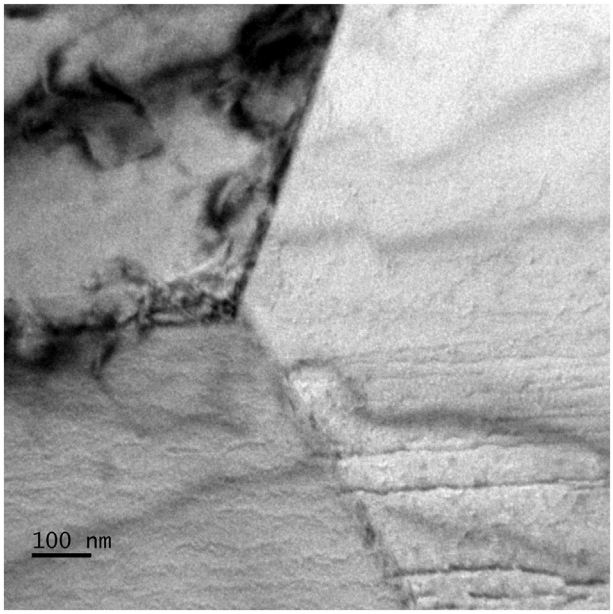

Fig. 2. Bright-field TEM micrograph from a depth more than 500 μm away from the top surface.

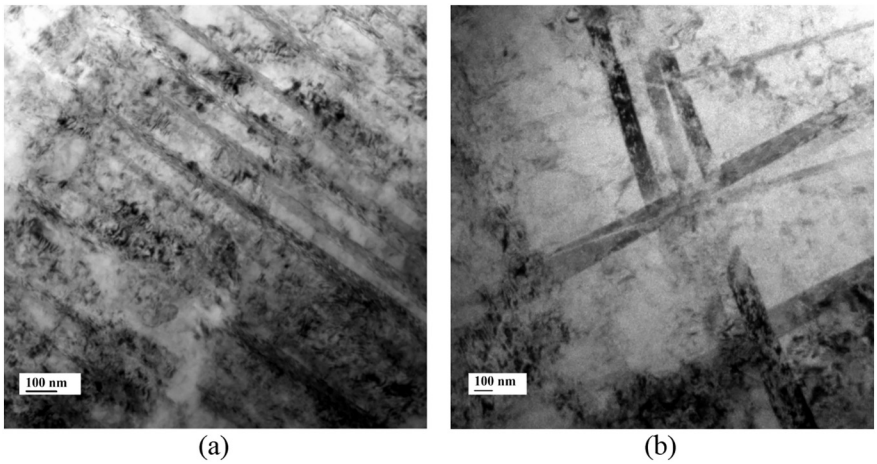

Fig. 3. Bright-field TEM micrographs from about 400–500 μm below the peened surface showing the presence of (a) shear bands and (b) multiple shear band intersections.

of size in the order of several micrometers are observed; which are separated by well-defined grain boundaries. It should be noted that the base material is a hot rolled sheet consisting of grains in the size range of 40–80 μm. This indicates that the microstructure below the GNS is essentially the microstructure of the base metal that is not largely affected by the peening process.

3.2. Microstructural features in the transition region

All the TEM micrographs in this section are from the transition region of the GNS layer. This region spans from about 20 μm to about 500 μm from the peened surface.

Fig. 3 depict the bright-field TEM micrographs of severe peened sample, from a region about 500 μm below the peened surface. Presence of mechanical twins, twin-twin intersections and huge amount of dislocations are observed in these micrographs. Similar deformation microstructures are observed by other researchers [5,16,21] upon severe peening of austenitic stainless steels. In the literature, different types of planar defects formed during the plastic deformation are collectively termed as “shear bands” [22,23]. Hence, the same term will be used in the further discussion. Number of shear bands and their intersections increase towards the peened surface owing to the multidirectional impact of shots on the surface encountered during the peening process [24]. Martensitic transformation is also observed in this region.

3.2.1. Deformation induced martensite formation

Upon severe shot peening, deformation induced transformation of austenite to martensite takes place. Depending on the chemistry of the steel and deformation conditions, austenite may directly transform to α′ martensite (having BCC structure) or through an intermediate phase called ε-martensite (having HCP structure). In the present study ε-martensite is not observed. It could be justified based on the observations in literature [23,25,26] where α′ martensite is directly nucleated on the intersecting shear bands of austenite.

Shear band formation takes place when austenitic stainless steel is subjected to deformation. It is largely advocated [16,27,28] that the deformation induced martensite (DIM) nucleates solely at shear band intersections during plastic deformation; while some researchers [29–31] have reported that they are merely the preferential sites for nucleation. It is reported [25] that any appropriate defect structure could serve as nucleation site for martensite nucleation. Through the in-situ TEM observations, Brooks et al. [26] have shown that the martensite always nucleates from the favourable dislocation configurations generated by the stress associated with the transformation. This affirms that the nucleation of DIM is not restricted to the shear band intersections. Also, there are reports in the literature [29,30,32] affirming the nucleation of DIM at grain boundaries. It is also reported that the martensite could form parallel to shear bands [24]. However, majority of the literature related to the mechanism of nanocrystallization in austenitic stainless steels upon severe peening, DIM nucleation is reported to be restricted to shear band intersections. In the present study,

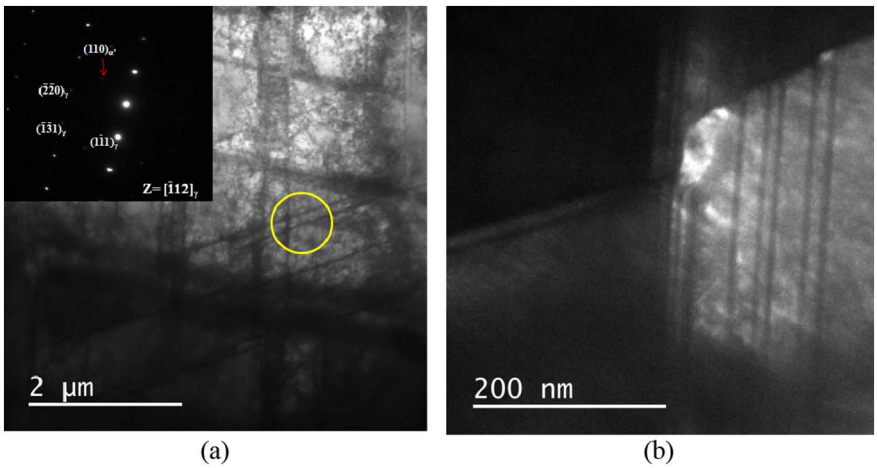

Fig. 4. (a) Bright-field TEM micrograph showing multiple shear band intersections. SAED from the marked region is given in the inset and (b) Dark-field TEM micrograph using (110) martensite reflection.

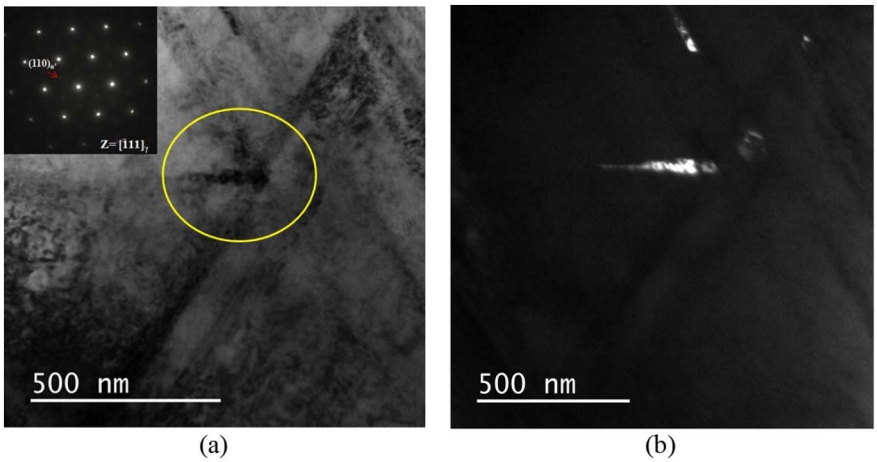

Fig. 5. (a) Bright-field TEM micrograph showing shear band intersection. SAED from the marked region in given in the inset and (b) Dark-field micrograph using (011) martensite reflection.

there are indications that DIM martensite has been nucleated at multiple locations in the austenite matrix as observed in the following TEM micrographs.

Bright-field TEM micrograph in Fig. 4(a) shows the austenite matrix with multiple shear band intersections. Selected area electron diffraction (SAED) pattern from the marked region is shown in the inset. Along with bright diffraction spots of austenite in [1̄12] zone axis, weaker martensite spots corresponding to [111] zone axis are also visible. Dark-field TEM micrograph from the (110) martensite reflection is given in Fig. 4(b). It could be clearly observed that martensite is nucleated at the shear band intersection [27,28].

The work of Murr et al. [24] suggests that the martensite nuclei formed at shear band intersections close to each other will impinge on each other. This results in the coalescence of martensite nuclei to form longer martensite laths. It is also justified by Lee et al [33] that martensite embryos overcoming the nucleation barrier will grow as long martensite laths until a barrier for the growth is encountered. It is illustrated by the bright-field TEM micrograph in Fig. 5(a). The SAED pattern from the marked region in the inset shows the spots corresponding to austenite ([1̄11] zone axis) and martensite ([111] zone axis). Dark-field micrograph in Fig. 5(b) from the (110) martensite reflection clearly shows the formation of martensite lath.

However, every shear band intersection need not be a nucleation site for the DIM transformation. It is reported [25,34] that critical nucleation size and strain invariant conditions should be satisfied at the shear band intersection to facilitate the martensite nucleation. Fig. 6(a) shows a typical bright-field TEM micrograph depicting the intersection of shear bands. Corresponding SAED pattern from the marked region is given in the inset. The diffraction spots correspond to [011] zone axis of the austenite phase with twin reflections. It suggests that, in the present case, shear bands are deformation twins in the austenite matrix. Dark-field TEM micrograph using the twin spot in the SAED is given in Fig. 6(b). No martensite is evident at the intersection.

In the study, it is observed that the martensite is nucleated in the locations other than the shear band intersections as well. Fig. 7(a) shows the presence of parallel shear bands in the austenite matrix and corresponding SAED pattern is given in the inset. Major spots in the SAED pattern correspond to austenite in [1̄12] zone axis while faint spots correspond to martensite in [111] orientation. The dark-field TEM micrograph from the (110) martensite reflection is given in Fig. 7(b). It could be observed that fine martensite units are formed parallel to the shear band. Width of the martensite formed is in the order of 10–20 nm.

Bright-field TEM micrograph in Fig. 8(a) depicts the presence of a shear band in the austenite matrix. SAED pattern from the marked region is given in the inset. Presence of a small unit of martensite could be observed inside the shear band. Diffraction spot corresponding to (110) plane of martensite is also observed in the SAED pattern. The dark-field TEM micrograph from (110) reflection of martensite is shown in Fig. 8(b) unambiguously confirms the unit as martensite.

Bright-field TEM micrograph in Fig. 9 shows the presence of parallel nano-scale shear bands in the austenite matrix. It could be observed that a martensite unit of about 150 nm is formed across these bands.

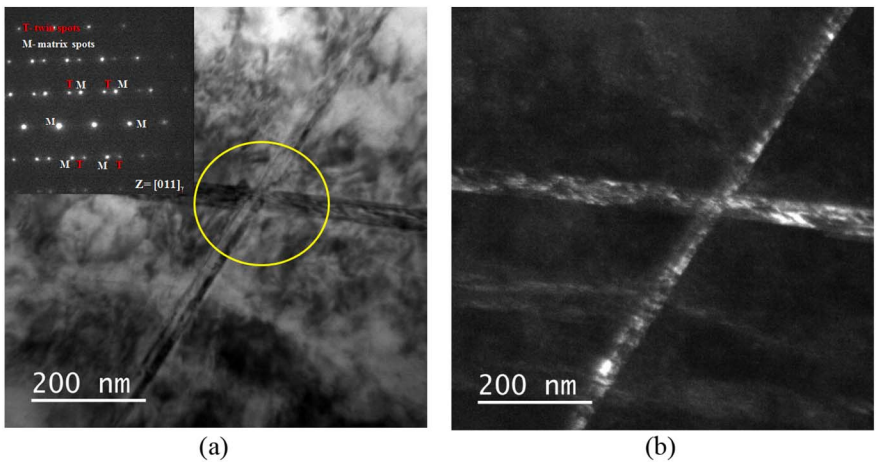

Fig. 6. (a) Bright-field TEM micrograph showing shearband intersection in the austenite and corresponding SAED pattern is given in the inset and (b) Dark-field TEM micrograph using twin spots.

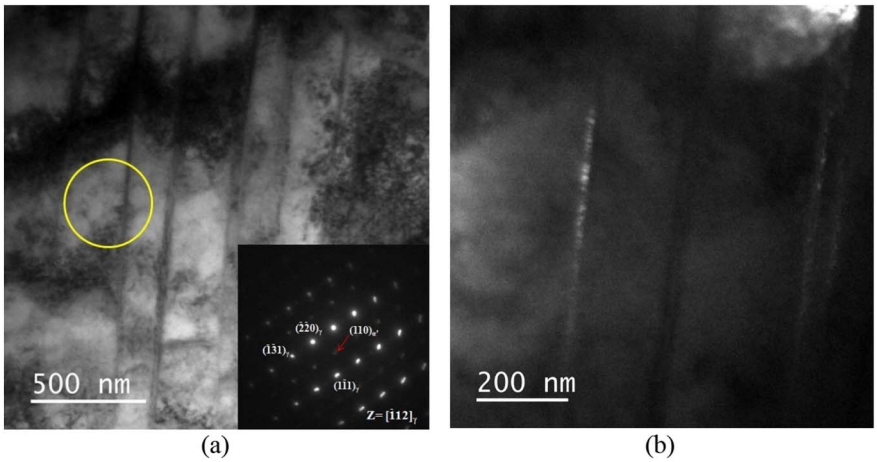

Fig. 7. (a) Bright-field TEM micrograph showing presence of parallel shear bands and SAED pattern from the marked region is given in the inset and (b) Higher magnification dark-field micrograph using (110) martensite reflection.

Convergent beam electron diffraction (CBED) pattern taken from the marked region is given in the inset and it corresponds to [111] zone axis of martensite. This suggests that martensite could also be formed across the nano-scale shear bands.

Fig. 10(a) is a bright-field TEM micrograph from the transition region of the GNS layer. SAED pattern from the marked region is given in the inset. SAED pattern consists of reflections from austenite as well as martensite phases. Dark-field TEM micrograph using (200) martensite reflection in Fig. 10(b) indicates the presence of lath martensite unit of about 200 nm thickness. Lower magnification dark-field TEM micrograph in Fig. 10(c) suggests that the martensite lath is closer to the grain boundary. This indicates that grain boundary could be the nucleation site for DIM transformation. There are reports in the literature [30,35] suggesting that martensite could nucleate at grain boundaries.

Bright-field TEM micrograph in Fig. 11(a) shows the presence of the parallel shear bands spaced few hundreds of nanometers apart in the austenite matrix. There are indications of nano-scale shear bands existing between these; along with the dislocations. SAED pattern taken from the area between two shear bands is given in the inset. Diffraction pattern corresponds to [$\bar{1}$12] zone axis of austenite while additional reflections are from the martensite phase. Higher magnification dark-field TEM micrograph using the (110) martensite reflection is given in Fig. 11(b). These micrographs affirm the presence of nano-scale shear bands between the major shear bands. Dark-field micrograph confirms the formation of DIM parallel to those nano-scale shear bands.

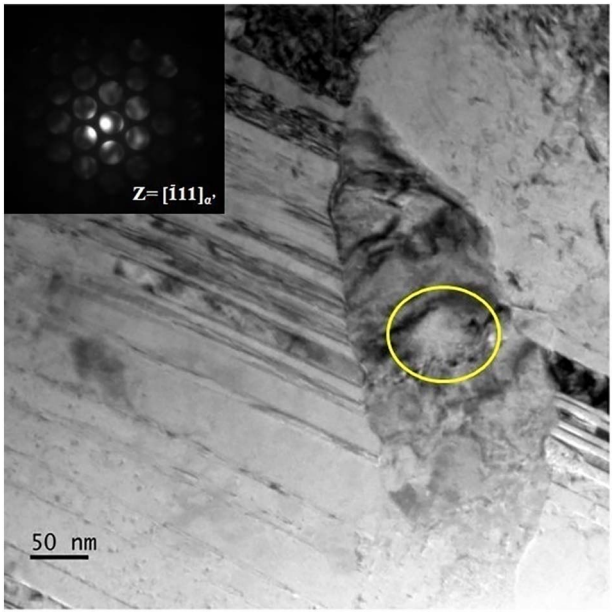

Fig. 9. Bright-field TEM micrograph showing the martensite unit formed across nano-scale shear bands. CBED pattern from the marked region is given in the inset.

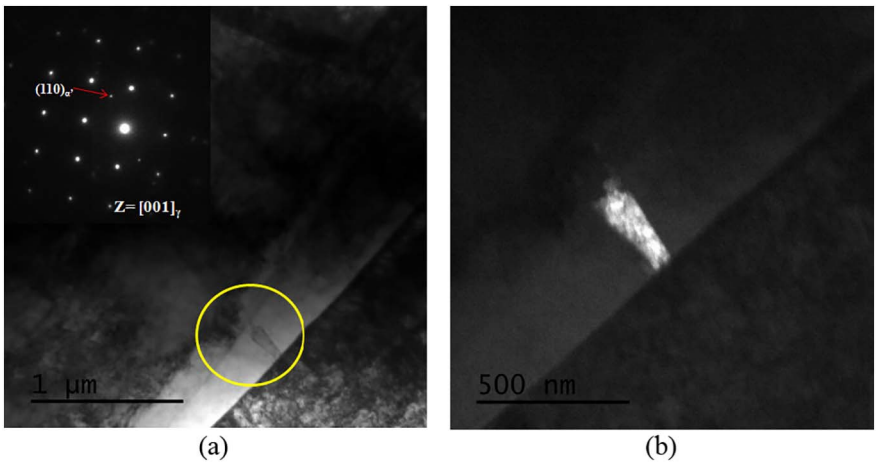

Fig. 8. (a) Bright-field TEM micrograph showing the presence of shear band in the austenite matrix. SAED pattern from the marked region is given in the inset and (b) Higher magnification dark-field TEM micrograph using (110) martensite reflection.

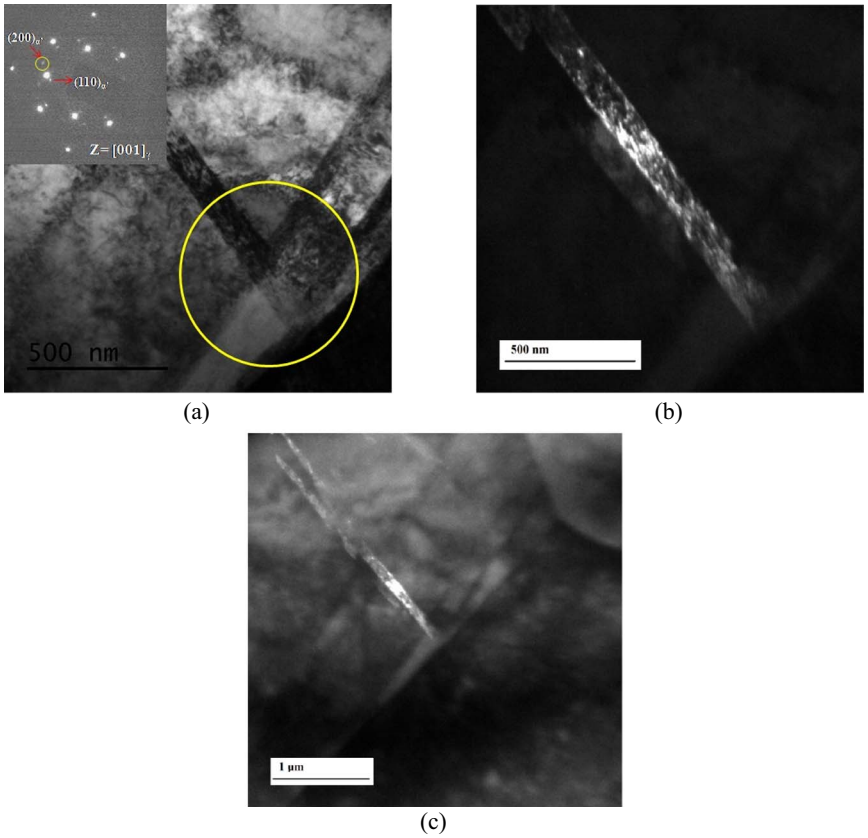

Fig. 10. (a) Bright-field TEM micrograph from transition region of GNS. SAED pattern from the marked region is in the inset (b) Dark-field TEM micrograph using (200) martensite reflection and (c) Lower magnification dark-field TEM micrograph showing the martensite unit at grain boundary.

3.3. Microstructural features in the nanocrystalline region

It is observed in the previous work [20] of authors that the nanocrystalline region of the GNS layer extends to about 20 μm from the top surface and it consists of martensite phase alone. However, it is observed that morphological features change from lath martensite to dislocation cell type martensite in this region. Fig. 12 shows the bright-field TEM micrographs from different layers in the nanocrystalline region.

The layer about 20 μm from the top surface (Fig. 12(a)) consists of lath martensite morphology. Individual laths are having thickness in the range of 80–120 nm while having length in the range of several micrometers. Huge amount of dislocations are found inside each lath. It should be noted that in the previous studies of surface nanostructuring of austenitic stainless steels through peening, formation of continuous layer of lath martensite is not reported. A report by Chen et al. [15] alone speaks about the formation lath martensite in 304SS during high speed SMAT process; however the laths formed are restricted to shear band intersection regions.

The layer above the lath martensite region (Fig. 12(b) and (c)) indicates the transition of martensite morphology from lath-type to dislocation cell-type. It could be observed that lath structure is getting broken as it is subjected to deformation at higher strain rate towards the surface. Hence, the dimensions of individual laths are decreasing

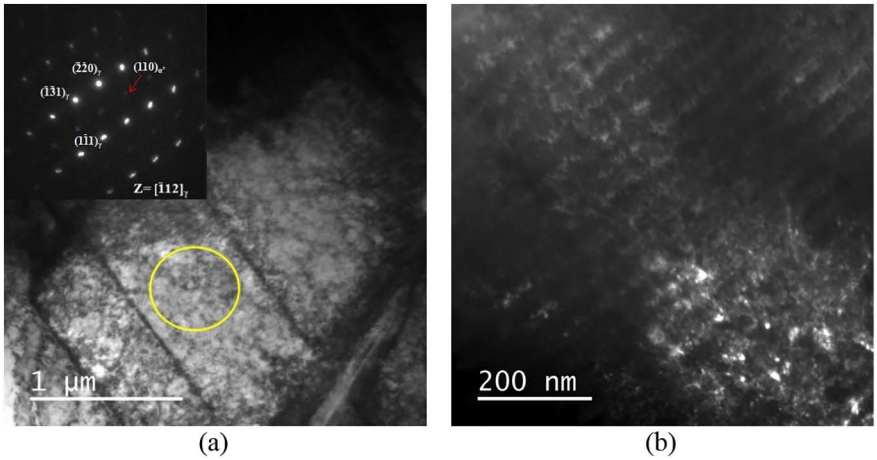

Fig. 11. (a) Bright-field TEM micrograph showing the presence of parallel shear bands. SAED pattern from the marked region is given in the inset and (b) Dark-field TEM micrograph using (110) martensite reflection.

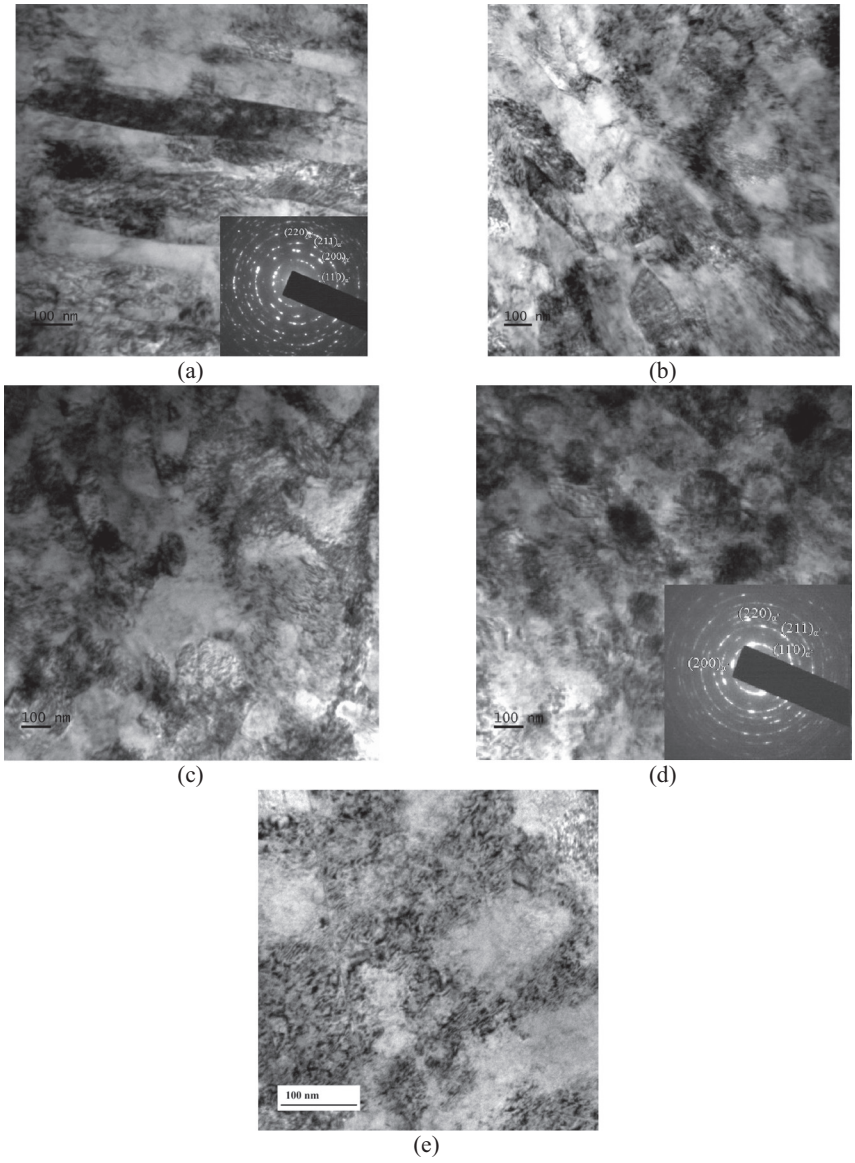

Fig. 12. Bright-field TEM micrographs from the nanocrystalline region of GNS showing (a) Lath martensite layer (b,c) transition from lath morphology to blocky morphology and (d,e) dislocation cell type martensite.

continuously. There is increase in the amount of dislocations and dislocation cells are emerging in certain locations of the microstructure. Similar structures are also observed by the other researchers upon severe shot peening [36] and ultrasonic impact treatment [37] of AISI 321 steel.

The microstructure at the top most surface is shown in Fig. 12(d). Higher magnification TEM micrograph is given in Fig. 12(e) which clearly exhibits the dislocation cell type morphology of the martensite. Martensite crystallites are nearly equiaxed; diameter in the range of 100–140 nm. The SAED pattern in the inset of Fig. 12(d) depicts continuous ring pattern from the martensite phase affirming that microstructure consists of randomly oriented fine martensite crystallites. This kind of transformation of morphology from lath to dislocation cell-type is also observed and reported by Mishra et al. [38] with increasing percentage reduction during cold rolling of AISI 301LN grade of stainless steel. However, it is also speculated [25] that the lath boundaries become unstable after growing to a critical dimension resulting in change of morphology from lath-type to blocky-type.

4. Conclusions

In summary, the transmission electron microscopic study of severe shot peened 316 SS reveals that,

- Severe shot peening generates about 500 μm thick gradient nanostructured (GNS) layer at the peened surface; refining the hot-rolled parent austenitic microstructure having grain size in the range of 40–80 μm to dislocation cell- type deformation induced martensitic structure of cell size in the range of 100–140 nm.
- Nucleation of DIM is not limited to shear band intersections. Martensite units found to nucleate at multiple locations in the austenite matrix; such as parallel to shear band, inside the shear band, across the shear band, near the grain boundaries, etc.
- Coalescence of martensite nuclei leads to formation of continuous layer of lath martensite at about 15–20 μm from the peened surface.
- Lath morphology changes over to dislocation cell type morphology due to breaking up of martensite laths by the high strain rate, multi-directional impact of shots at the topmost surface.

Acknowledgements

We would like to acknowledge the Director, NITK and MHRD, Govt. of India for providing financial assistance for this research work.

References

[1] S. Bagheri, M. Guagliano, Review of shot peening processes to obtain nanocrystalline surfaces in metal alloys, Surf. Eng. 25 (2009) 3–14, http://dx.doi.org/10.1179/026708408X334087.
[2] J.L. Liu, M. Umemoto, Y. Todaka, K. Tsuchiya, Formation of a nanocrystalline surface layer on steels by air blast shot peening, J. Mater. Sci. 42 (2007) 7716–7720, http://dx.doi.org/10.1007/s10853-007-1659-x.
[3] S.M. Hassani-Gangaraj, K.S. Cho, H.J.L. Voigt, M. Guagliano, C.A. Schuh, Experimental assessment and simulation of surface nanocrystallization by severe shot peening, Acta Mater. 97 (2015) 105–115, http://dx.doi.org/10.1016/j.actamat.2015.06.054.
[4] G. Liu, J. Lu, K. Lu, Surface nanocrystallization of 316L stainless steel induced by ultrasonic shot peening, Mater. Sci. Eng. A 286 (2000) 91–95, http://dx.doi.org/10.1016/S0921-5093(00)00686-9.
[5] J.Z. Lu, K.Y. Luo, Y.K. Zhang, G.F. Sun, Y.Y. Gu, J.Z. Zhou, X.D. Ren, X.C. Zhang, L.F. Zhang, K.M. Chen, C.Y. Cui, Y.F. Jiang, A.X. Feng, L. Zhang, Grain refinement mechanism of multiple laser shock processing impacts on ANSI 304 stainless steel, Acta Mater. 58 (2010) 5354–5362, http://dx.doi.org/10.1016/j.actamat.2010.06.010.
[6] T. Balusamy, T.S.N.S. Narayanan, K. Ravichandran, I.S. Park, M.H. Lee, Plasma nitriding of AISI 304 stainless steel: role of surface mechanical attrition treatment, Mater. Charact. 85 (2013) 38–47, http://dx.doi.org/10.1016/j.matchar.2013.08.009.
[7] N. Tsuji, S. Tanaka, T. Takasugi, Effects of combined plasma-carburizing and shot-peening on fatigue and wear properties of Ti-6Al-4V alloy, Surf. Coat. Technol. 203 (2009) 1400–1405, http://dx.doi.org/10.1016/j.surfcoat.2008.11.013.
[8] A. Başaran, N. Kurgan, R. Varol, Investigation of fatigue properties of shot peened and plasma nitrocarburized P/M FC0205 steel, J. Mech. Sci. Technol. 27 (2013) 2315–2322, http://dx.doi.org/10.1007/s12206-013-0615-8.
[9] H.P. Yang, X.C. Wu, Y.A. Min, T.R. Wu, J.Z. Gui, Plasma boriding of high strength alloy steel with nanostructured surface layer at low temperature assisted by air blast shot peening, Surf. Coat. Technol. 228 (2013) 229–233, http://dx.doi.org/10.1016/j.surfcoat.2013.04.033.
[10] L. Shen, L. Wang, Y. Wang, C. Wang, Plasma nitriding of AISI 304 austenitic stainless steel with pre-shot peening, Surf. Coat. Technol. 204 (2010) 3222–3227, http://dx.doi.org/10.1016/j.surfcoat.2010.03.018.
[11] S. Bagherifard, S. Slawik, I. Fernández-Pariente, C. Pauly, F. Mücklich, M. Guagliano, Nanoscale surface modification of AISI 316L stainless steel by severe shot peening, Mater. Des. 102 (2016) 68–77, http://dx.doi.org/10.1016/j.matdes.2016.03.162.
[12] H.W. Huang, Z.B. Wang, J. Lu, K. Lu, Fatigue behaviors of AISI 316L stainless steel with a gradient nanostructured surface layer, Acta Mater. 87 (2015) 150–160, http://dx.doi.org/10.1016/j.actamat.2014.12.057.
[13] Y.G. Liu, M.Q. Li, H.J. Liu, Surface nanocrystallization and gradient structure developed in the bulk TC4 alloy processed by shot peening, J. Alloys Compd. 685 (2016) 186–193, http://dx.doi.org/10.1016/j.jallcom.2016.05.295.
[14] Y.G. Liu, M.Q. Li, H.J. Liu, Nanostructure and surface roughness in the processed surface layer of Ti-6Al-4V via shot peening, Mater. Charact. 123 (2017) 83–90, http://dx.doi.org/10.1016/j.matchar.2016.11.020.
[15] A.Y. Chen, H.H. Ruan, J. Wang, H.L. Chan, Q. Wang, Q. Li, J. Lu, The influence of strain rate on the microstructure transition of 304 stainless steel, Acta Mater. 59 (2011) 3697–3709, http://dx.doi.org/10.1016/j.actamat.2011.03.005.
[16] H.W. Zhang, Z.K. Hei, G. Liu, J. Lu, K. Lu, Formation of nanostructured surface layer on AISI 304 stainless steel by means of surface mechanical attrition treatment, Acta Mater. 51 (2003) 1871–1881, http://dx.doi.org/10.1016/S1359-6454(02)00594-3.
[17] L. Zhou, W. He, S. Luo, C. Long, C. Wang, X. Nie, G. He, X. Shen, Y. Li, Laser shock peening induced surface nanocrystallization and martensite transformation in austenitic stainless steel, J. Alloys Compd. 655 (2016) 66–70, http://dx.doi.org/10.1016/j.jallcom.2015.06.268.
[18] S. Bahl, S. Suwas, T. Ungàr, K. Chatterjee, Elucidating microstructural evolution and strengthening mechanisms in nanocrystalline surface induced by surface mechanical attrition treatment of stainless steel, Acta Mater. 122 (2017) 138–151 (doi: 10.1016/j.actamat.2016.09.041).
[19] M. Jayalakshmi, B. Ramachandra Bhat, K. Udaya Bhat, Effect of shot peening coverage on surface nanostructuring of 316L stainless steel and its influence on low temperature plasma-nitriding, Mater. Perform. Charact. 6 (2017), http://dx.doi.org/10.1520/MPC20160079.
[20] M. Jayalakshmi, P. Huilgol, B.R. Bhat, K.U. Bhat, Microstructural characterization of low temperature plasma-nitrided 316L stainless steel surface with prior severe shot peening, JMADE. 108 (2016) 448–454, http://dx.doi.org/10.1016/j.matdes.2016.07.005.
[21] N.R. Tao, H. Zhang, J. Lu, K. Lu, Development of nanostructures in metallic materials with low stacking fault energies during surface mechanical attrition treatment (SMAT), Mater. Trans. 44 (2003) 1919–1925, http://dx.doi.org/10.2320/matertrans.44.1919.
[22] G.B. Olson, M. Cohen, Kinetics of strain-induced martensitic nucleation, Metall. Trans. A. 6 (1975) 791–795, http://dx.doi.org/10.1007/BF02672301.
[23] J. Talonen, H. Hänninen, Formation of shear bands and strain-induced martensite during plastic deformation of metastable austenitic stainless steels, Acta Mater. 55 (2007) 6108–6118, http://dx.doi.org/10.1016/j.actamat.2007.07.015.
[24] L.E. Murr, K.P. Staudhammer, S.S. Hecker, Effects of strain state and strain rate on deformation-induced transformation in 304 stainless steel: part II. Microstructural study, Metall. Trans. A. 13 (1982) 627–635, http://dx.doi.org/10.1007/BF02644428.
[25] V. Shrinivas, S.K. Varma, L.E. Murr, Deformation-induced martensitic characteristics in 304 and 316 stainless steels during room-temperature rolling, Metall. Mater. Trans. A 26 (1995) 661–671, http://dx.doi.org/10.1007/BF02663916.
[26] J.W. Brooks, M.H. Loretto, R.E. Smallman, In situ observations of the formation of martensite in stainless steel, Acta Metall. 27 (1979) 1829–1838, http://dx.doi.org/10.1016/0001-6160(79)90073-7.
[27] G.B. Olson, A mechanism for the strain-induced nucleation of martensitic transformations, J. Less-Common Met. 28 (1972) 107–118, http://dx.doi.org/10.1016/0022-5088(72)90173-7.
[28] F. Lecroise, A. Pineau, Martensitic transformations induced by plastic-deformation in Fe-Ni-Cr-C system, Metall. Trans. A. 3 (1972) 387–396.
[29] Y.E. Tian, O.I. Gorbatov, A. Borgenstam, A.V. Ruban, P. Hedström, Deformation microstructure and deformation-induced martensite in austenitic Fe-Cr-Ni alloys depending on stacking fault energy, Metall. Mater. Trans. A 48 (2017) 1–7, http://dx.doi.org/10.1007/s11661-016-3839-2.
[30] A. Das, S. Sivaprasad, M. Ghosh, P.C. Chakraborti, S. Tarafder, Morphologies and characteristics of deformation induced martensite during tensile deformation of 304 LN stainless steel, Mater. Sci. Eng. A 486 (2008) 283–286, http://dx.doi.org/10.1016/j.msea.2007.09.005.
[31] N. Gey, B. Petit, M. Humbert, Electron backscattered diffraction study of ε/α′ martensitic variants induced by plastic deformation in 304 stainless steel, Metall. Mater. Trans. A 36 (2005) 3291–3299, http://dx.doi.org/10.1007/s11661-005-0003-9.
[32] M.N. Gussev, J.T. Busby, T.S. Byun, C.M. Parish, Twinning and martensitic transformations in nickel-enriched 304 austenitic steel during tensile and indentation deformations, Mater. Sci. Eng. A 588 (2013) 299–307, http://dx.doi.org/10.1016/j.msea.2013.08.072.
[33] W.-S. Lee, C.-F. Lin, Effects of prestrain and strain rate on dynamic deformation characteristics of 304L stainless steel: part 2 - microstructural study, Mater. Sci. Technol. 18 (2002) 869–876 (doi: 10.1179/026708302225004720).
[34] L.E. Murr, S.S. Hecker, K.P. Staudhammer, Nucleation and evolution of strain-induced martensitic (B.C.C.) embryos and substructure in stainless steel: a transmission electron microscope study, Acta Metall. 31 (1983) 267–274.
[35] R. Naraghi, P. Hedström, A. Borgenstam, Spontaneous and deformation-induced martensite in austenitic stainless steels with different stability, Steel Res. Int. 82 (2011) 337–345, http://dx.doi.org/10.1002/srin.201000118.
[36] S. Pour-Ali, A.R. Kiani-Rashid, A. Babakhani, S. Virtanen, M. Allieta, Correlation between the surface coverage of severe shot peening and surface microstructural evolutions in AISI 321: a TEM, FE-SEM and GI-XRD study, Surf. Coat. Technol. 334 (2018) 461–470, http://dx.doi.org/10.1016/j.surfcoat.2017.11.062.
[37] M.A. Vasylyev, B.N. Mordyuk, S.I. Sidorenko, S.M. Voloshko, A.P. Burmak, Influence of microstructural features and deformation-induced martensite on hardening of stainless steel by cryogenic ultrasonic impact treatment, Surf. Coat. Technol. (2017), http://dx.doi.org/10.1016/j.surfcoat.2017.11.019.
[38] R.D.K. Misra, S. Nayak, S.A. Mali, J.S. Shah, M.C. Somani, L.P. Karjalainen, On the significance of nature of strain-induced martensite on phase-reversion-induced nanograined/ultrafine-grained austenitic stainless steel, Metall. Mater. Trans. A Phys. Metall. Mater. Sci. 41 (2010) 3–12, http://dx.doi.org/10.1007/s11661-009-0072-2.